Journal of The Electrochemical Society

OPEN ACCESS

Comparative Study of PEDOT- and PEDOT:PSS Modified δ-MnO_2 Cathodes for Aqueous Zinc Batteries with Enhanced Properties

To cite this article: M. A. Kamenskii *et al* 2023 *J. Electrochem. Soc.* **170** 010505

Journal of The Electrochemical Society, 2023 **170** 010505

Comparative Study of PEDOT- and PEDOT:PSS Modified δ-MnO_2 Cathodes for Aqueous Zinc Batteries with Enhanced Properties

M. A. Kamenskii,[1] F. S. Volkov,[1] S. N. Eliseeva,[1] R. Holze,[1,2,3,*] and V. V. Kondratiev[1,z]

[1]*Department of Electrochemistry, Institute of Chemistry, Saint Petersburg State University 7/9 Universitetskaya nab., St. Petersburg, 199034, Russia*
[2]*Institut für Chemie, Technische Universität Chemnitz, 09107 Chemnitz, Germany*
[3]*State Key Laboratory of Materials-oriented Chemical Engineering, School of Energy Sci-ence and Engineering, Nanjing Tech University, Nanjing, 211816, Jiangsu Province, People's Republic of China*

Chemically synthesized layered manganese dioxide (δ-MnO_2) modified by poly(3,4-ethylenedioxythiophene) (PEDOT) and poly (3,4-ethylenedioxythiophene):polystyrene sulfonate (PEDOT:PSS) dispersion were used as cathode materials for aqueous Zn-ion batteries (AZIBs). A comparative study of electrochemical properties of cathodes with pristine MnO_2 and materials chemically modified by conducting polymers in different forms was performed with cycling voltammetry and galvanostatic charge-discharge curves in Zn^{2+}-containing electrolyte solutions. The results of electrochemical tests indicate the significant improvement in specific capacity of electrodes in the sequence MnO_2, MnO_2/PEDOT and MnO_2/PEDOT:PSS composites. The MnO_2/PEDOT:PSS electrode delivered a specific discharge capacity of 278 mAh·g^{-1} at a current density 0.3 A·g^{-1} after 100 cycles, whereas for MnO_2/PEDOT and MnO_2 electrodes the values were 238 and 121 mAh·g^{-1} (capacity retention is 99%, 99.5% and 89%, respectively). These specific capacity values obtained for manganese dioxide-based cathodes are demonstrating the positive role of intrinsically conducting polymer, especially in case of surface modification of electroactive particles by PEDOT:PSS dispersion.
 [DOI: 10.1149/1945-7111/acabec]

Manuscript submitted June 15, 2022; revised manuscript received December 1, 2022. Published January 9, 2023.

Supplementary material for this article is available online

Increasing demand for portable electronic devices, electric vehicles and stationary energy storage systems is a driving force for active development of novel types of electrochemical power sources. Although lithium-ion batteries are still the most widely used electrochemical storage devices, in the last years another research focus is concentrated on aqueous zinc-ion batteries (AZIBs) due to the abundance of zinc, their environmental friendliness, safety and low cost.[1,2] As with lithium-ion batteries, several types of cathodes were proposed for AZIBs. Among them, manganese dioxide MnO_2 is considered as a promising eco-friendly material because of its high variety of polymorphic phases which allow constructing materials with a given morphology, relatively high theoretical specific capacity (308 mAh·g^{-1}) and high discharge electrode potential (≈1.4 V vs Zn/Zn^{2+}).[3–7]

Layered-type manganese dioxide (δ-MnO_2) has the largest interlayer distance up to 7 Å which allows zinc ions to intercalate in this lattice reversibly. This leads to improved cycling performance of δ-MnO_2-based cathodes in AZIBs.[3,7–10] Nevertheless, major drawbacks of manganese-based materials are poor electronic conductivity (close to 10^{-6} Sm·cm^{-1}) and fast capacity fading during cycling. This is caused by manganese dissolution in the discharge state (fast Mn^{3+} - Mn^{2+} transfer) and leads to structural instability of the material.[11] To suppress the Mn^{2+} release, addition of manganese salt to the electrolyte is usually applied.

To overcome the poor electronic contact and improve the electrochemical performance, different types of conducting coatings can be applied. This allows not only enhancing the conductivity of the composite material, but also diminishes the manganese dissolution due to addition of a physical barrier on active grains. The application of several intrinsically conducting polymers ICPs like polypyrrole,[12,13] polyaniline[14,15] and poly-3.4-ethylene-dioxy-thio-phene[16,17] was recently reported which resulted in an improvement of electrochemical properties. It should be noted that the use of ICPs allow the development of flexible quasi-solid cells and devices.

This work aims at a comparison of the electrochemical performance of δ-MnO_2 electrode materials obtained by modification of the same initial powder with the ICP poly-3,4-ethylenedioxythiophene (PEDOT) and dispersion of PEDOT with polystyrene sulfonate anion (PEDOT:PSS) in the mildly neutral electrolyte 2 M $ZnSO_4$ and 0.1 M $MnSO_4$. It was previously shown that at low current densities PEDOT additive has a positive influence on the electrochemical properties of δ-MnO_2 cathodes cast on carbon paper.[18] Here, a more detailed study of electrochemical properties of composite materials with different forms of PEDOT was performed.

It was demonstrated that the use of PEDOT:PSS for surface modification yielded a high discharge capacity of 302 and 280 mAh·g^{-1} at current densities 0.1 and 0.3 A·g^{-1}, respectively (based on the MnO_2 mass of the cathode), thus outperforming many recently reported results for Zn–MnO_2 aqueous batteries. Moreover, for the MnO_2/PEDOT:PSS cathode an excellent capacity retention (99%) was obtained during 100 charge/discharge cycles.

Experimental

Materials and electrodes preparation.—The δ-MnO_2 powder was synthesized by a hydrothermal method similar to the one described in Ref. 19. 0.949 g of $KMnO_4$ was dissolved in 50 ml of deionized water. Thereafter 0.151 g $MnSO_4$ was added. The obtained solution was vigorously stirred at room temperature for 30 min, then transferred into a PTFE-lined autoclave and heated up to 160 °C for 12 h. The obtained dark powder was washed with deionized water several times, then it was dried under vacuum (1 mbar) at 60 °C overnight. The obtained product was examined with X-ray diffraction measurements (XRD, Bruker-AXS D8 DISCOVER, Germany) using Cu Kα radiation and scanning electron microscopy (SEM, SUPRA 40VP Carl Zeiss, Germany).

Poly(3,4-ethylenedioxythiophene) (PEDOT) was prepared by chemical oxidation of monomer 3,4-ethylenedioxythiophene (EDOT) in the presence of $FeCl_3$. 200 ml of 0.07 M $FeCl_3$/acetonitrile solution was added in a round-bottom glass flask and stirred at 1000 rpm. Then,

*Electrochemical Society Member.
[z]E-mail: v.kondratev@spbu.ru

2 ml of EDOT were added dropwise under stirring. The resulting solution was stirred for 2 h. The obtained product was washed with acetonitrile and deionized water several times and dried at 80 °C for constant weight and characterized by SEM with energy dispersive X-ray analysis (EDX).

δ-MnO_2 composite material with poly(3,4-etylenedioxythiophene):polystyrene sulfonate (PEDOT:PSS) coating was prepared by mechanical mixing of δ-MnO_2 powder in aqueous dispersion of PEDOT:PSS (1.3 wt%, Aldrich) for 1 h and slow evaporation of water at 70 °C.

Three types of electrode materials were prepared by mechanical mixing of δ-MnO_2 powder with carbon black, PEDOT and polyvinylidene fluoride (PVDF) in the mass ratio presented in Table I. The resulting viscous slurries were casted onto a Ti foil (blade gap height = 150 μm) and dried under vacuum at 60 °C overnight.

Electrochemical measurements.—Electrodes were assembled in CR2032 coin cells with a Zn anode and 2 M $ZnSO_4$/0.1 M $MnSO_4$ aqueous electrolyte and preliminary soaked Whatman GF/A glass fiber as separator. The electrochemical performance tests were made by galvanostatic charge-discharge (GCD) and cyclic voltammetry (CV) in the potential range 1.0–1.8 V vs Zn/Zn^{2+} electrode. GCD tests were performed on an automatic galvanostatic charge-discharge battery cell test instrument CT-4008 (Neware Co., China) at 0.1 $A{\cdot}g^{-1}$–5 $A{\cdot}g^{-1}$ current rates at room temperature (20 ± 2 °C). CV measurements were carried out on a potentiostat/galvanostat BioLogic BT-805 (France) at scan rates in the range of 0.1–0.5 $mV{\cdot}s^{-1}$.

Results and Discussion

Figure 1a presents XRD patterns of as-synthesized δ-MnO_2 powder. Very intense peaks at 12.46° and 25.09° are observed with several coupled and low-intensity peaks which are typically observed for layered-type materials. These diffraction peaks can be indexed to monoclinic potassium-doped birnessite 2H phase with molecular formula $K_{0.46}Mn_2O_4 \cdot 1.55\ H_2O$ matching the ICCD card no. 01–75–8312. This finding is in close agreement with reported chemical formulae of layered-type manganese dioxide, synthesized by the same procedure.[19]

In the SEM images of the powder (Fig. 1b) nanoflower-like MnO_2 is observed as agglomerated grains with highly porous morphology. A tendency to the formation of separated layers is also noticed. The ratio Mn:O observed from EDX analysis (Table SI) is close to 1:1.8.

SEM images of PEDOT powder demonstrate that highly porous amorphous structures are observed with additional ideal spheres (Fig. 2a). From the EDX analysis ratio of components is close to the theoretical for PEDOT (Table SII).

In the SEM images of the electrode materials a more dense and smooth surface is observed for PEDOT-containing electrodes, especially for MnO_2/PEDOT:PSS electrode, in comparison with bare MnO_2 electrode (Figs. 2b–2d). From the EDX analysis for all three electrode materials the manganese and oxygen distributions are uniform. The sulphur distribution in MnO_2/PEDOT electrode is also well-random (Fig. S4) and in case of MnO_2/PEDOT:PSS electrode it is uniform but in correlation with manganese presence (Fig. S5). Thus, the addition of ICP dispersion allows us to obtain a novel type of MnO_2-based cathode material, covered with polymer.

Electrochemical properties of all types of prepared electrodes were evaluated by cyclic voltammetry and galvanostatic charge/discharge.

Figure 3 shows the cyclic voltammograms of MnO_2-based cathodes. In general, CV shapes for different cathodes were very similar and they displayed two redox couples which are typical for Zn/δ-MnO_2 system and agree with literature data.[8,20,21] Two cathodic peaks located at $E = 1.37$ and $E = 1.24$ V correspond to reduction of Mn^{4+} to Mn^{3+}; they are accompanied by intercalation of protons (1.37 V) and of Zn^{2+} ions (1.24 V). The interpretation of the electrode process at the second peak (1.24 V) is more debatable, the peak is commonly assigned to Zn^{2+} intercalation, complicated by chemical formation of byproducts like zinc sulfate hydroxide $Zn_4(OH)_6SO_4{\cdot}xH_2O$ (ZHS) during the cathodic process at E = 1.24 V.[22] A detailed study of electrochemical reactions was performed with quartz microgravimetric analysis.[23] The magnitude of apparent molar mass of species transferred is approximately proportional to the molecular mass of H_3O^+ ions for the first peak (E = 1.4 V) and significantly higher than the molecular mass of Zn^{2+} ions for the second peak (E = 1.26 V). Based on the molecular weights of species taken into account in the redox process, the first peak was attributed to intercalation of H^+ (as H_3O^+) and the second peak is related to precipitation of ZHS with Zn^{2+}-intercalation which was also assumed in Ref. 24 for a $Zn(TFSI)_2$-based electrolyte.

Two not well-resolved anodic peaks at $E = 1.56$ and $E = 1.62$ V were observed which are related to Mn^{3+}-ion oxidation with corresponding extraction of zinc ions and protons, respectively. Both cathodic and anodic peaks gradually increased with the number of cycles, indicating the progressive electrodeposition of newly formed MnO_x or ε-MnO_2 layers onto electrode surface from Mn^{2+} ions contained in the electrolyte solution.

The discharge capacities from the CV curves are a little higher for MnO_2/PEDOT and MnO_2/PEDOT:PSS electrodes because of the widening of the cathodic peaks, especially the second one, which could be associated with progressive ZHS precipitation on the more porous surface and formation of "diffusion valleys." During charge, a gradual capacity increase is observed due to the presence of Mn^{2+} ions and MnO_x layers deposited on the electrode surface.

With increasing scan rate (from 0.2 $mV{\cdot}s^{-1}$ to 0.5 $mV{\cdot}s^{-1}$) for all three electrodes the pair of cathodic and anodic peaks associated with zinc ion insertion/extraction are significantly diminished (Figs. 4a, S6). It is clearer for the cathodic curve, where the second reduction peak completely disappeared at high scan rates. So, this allows us to suppose that at high scan rates insertion and extraction of protons become the dominant redox processes.

From the double logarithmic plot for MnO_2/PEDOT:PSS electrode (Fig. 4b), the slopes of the lgI_p, $lg\nu$-dependencies are 0.64 and 0.71. Based on general descriptions, both diffusion-controlled and pseudocapacitive currents may flow. The experimental data will obey an empirical equation, in which the dependency of peak currents on the scan rate is a power function:

$$I_p = a{\cdot}\nu^b, \qquad [1]$$

with I_p—peak current, ν—scan rate, b—the exponent. This equation can be rewritten in logarithmic form

Table I. δ-MnO_2-based electrodes composition (in wt%).

Sample	δ-MnO_2	C	PVDF	PEDOT	PEDOT:PSS
δ-MnO_2	70	20	10	0	0
δ-MnO_2/PEDOT	68	20	7	5	0
δ-MnO_2/PEDOT:PSS	70	20	8	0	2

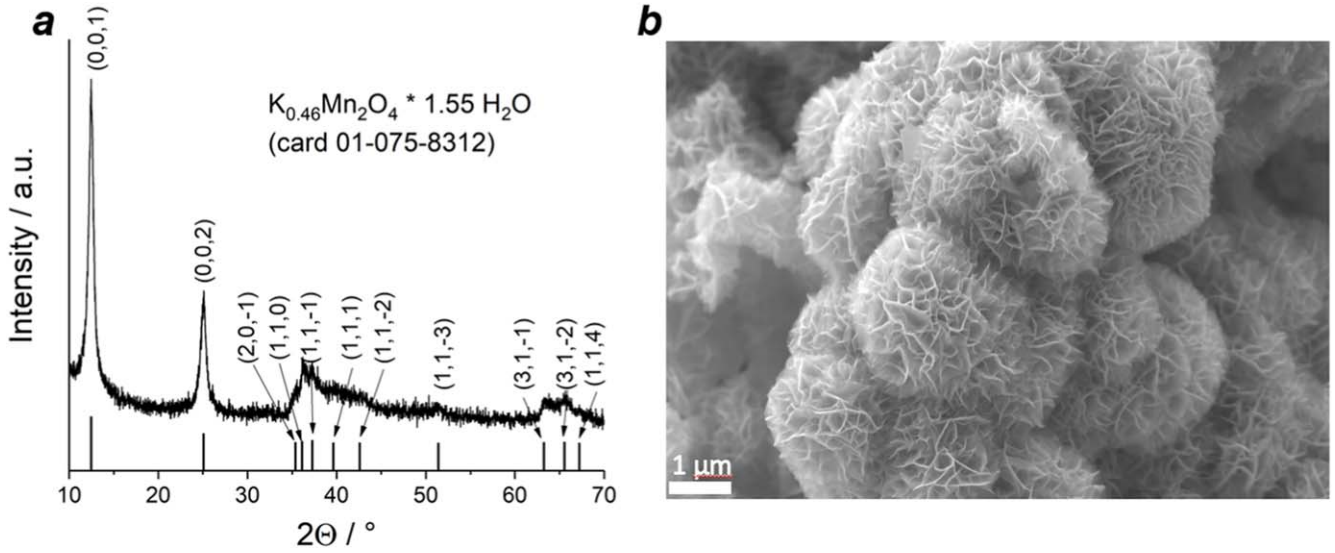

Figure 1. (a) XRD patterns and (b) SEM image of δ-MnO_2 powder.

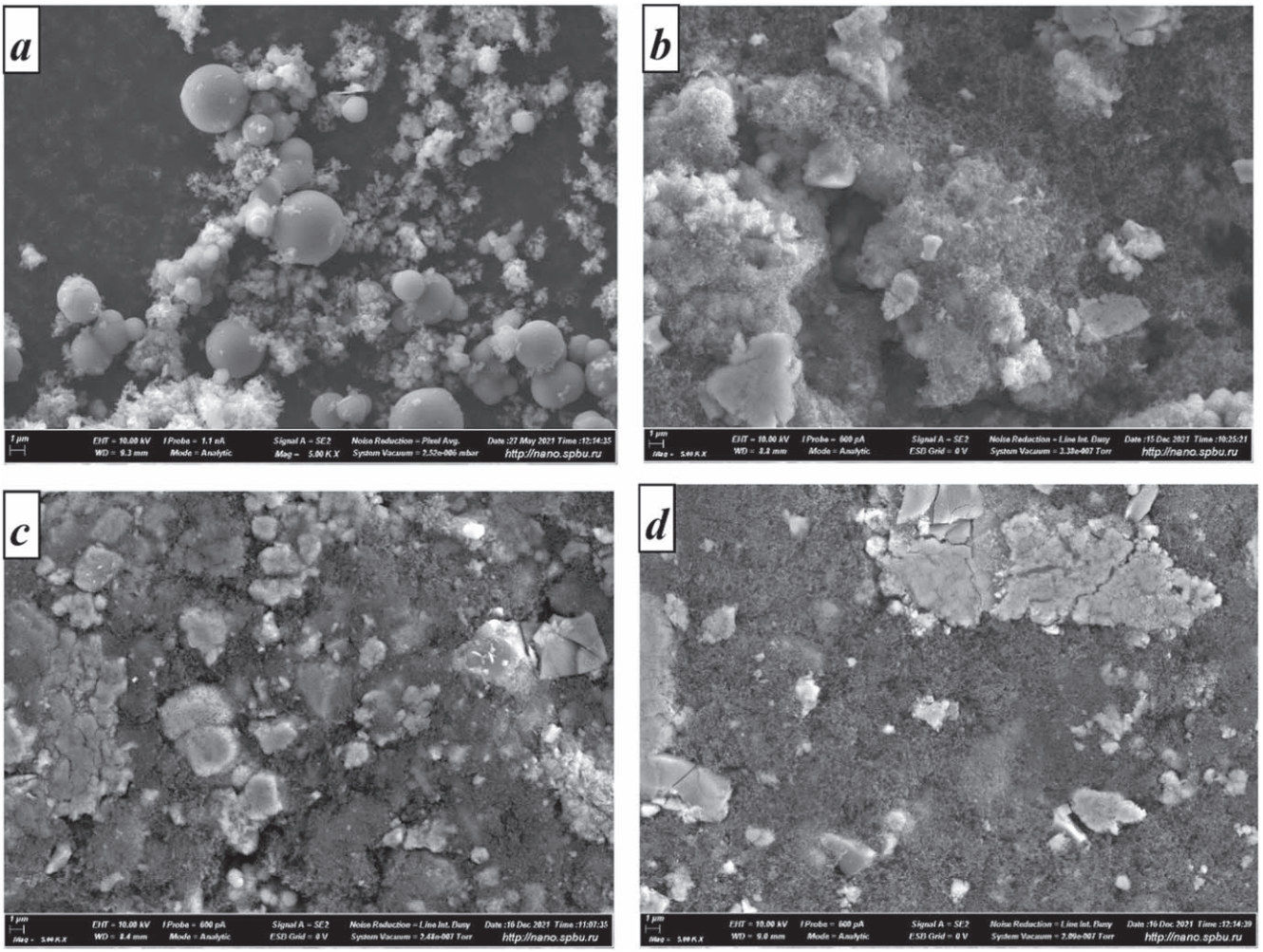

Figure 2. SEM images of PEDOT powder (a) and three types of MnO_2-based electrodes: without conducting polymer (b), with addition of PEDOT (c) and coated with PEDOT:PSS (d).

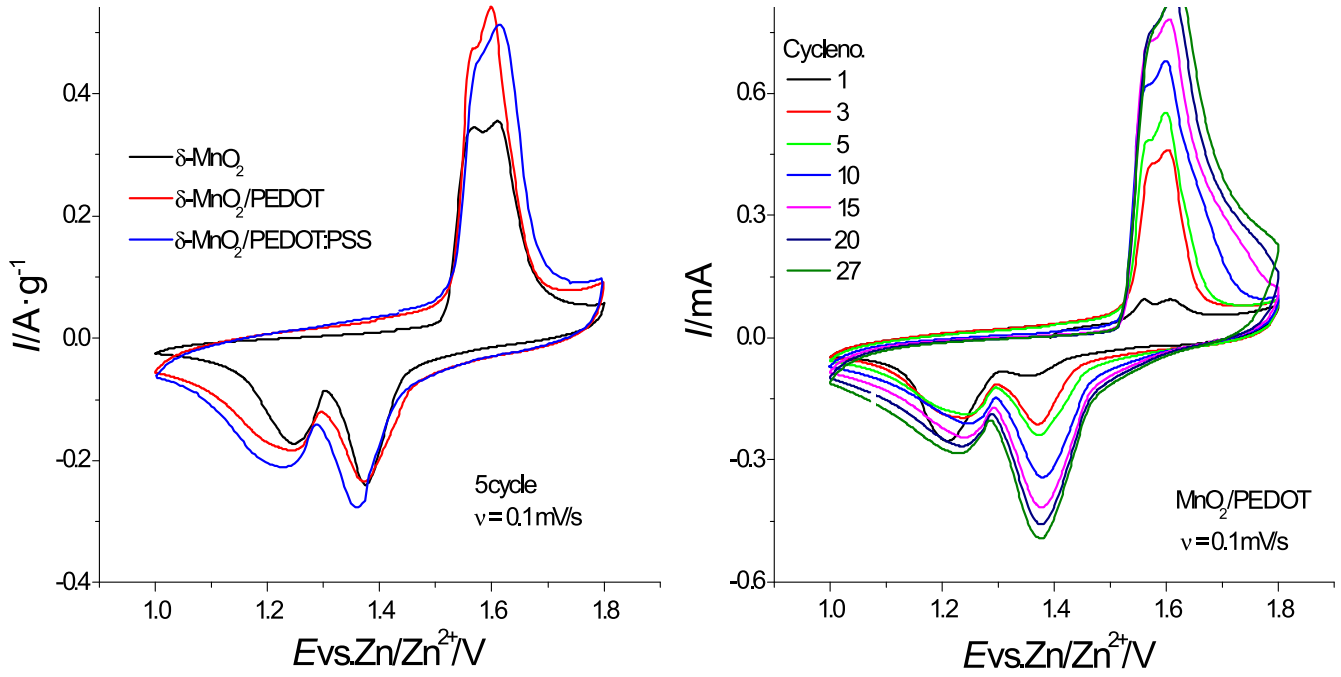

Figure 3. Cyclic voltammograms of MnO_2-based electrodes at a scan rate of 0.1 $mV{\cdot}s^{-1}$ (a) and a MnO_2/PEDOT electrode at various cycle numbers (b).

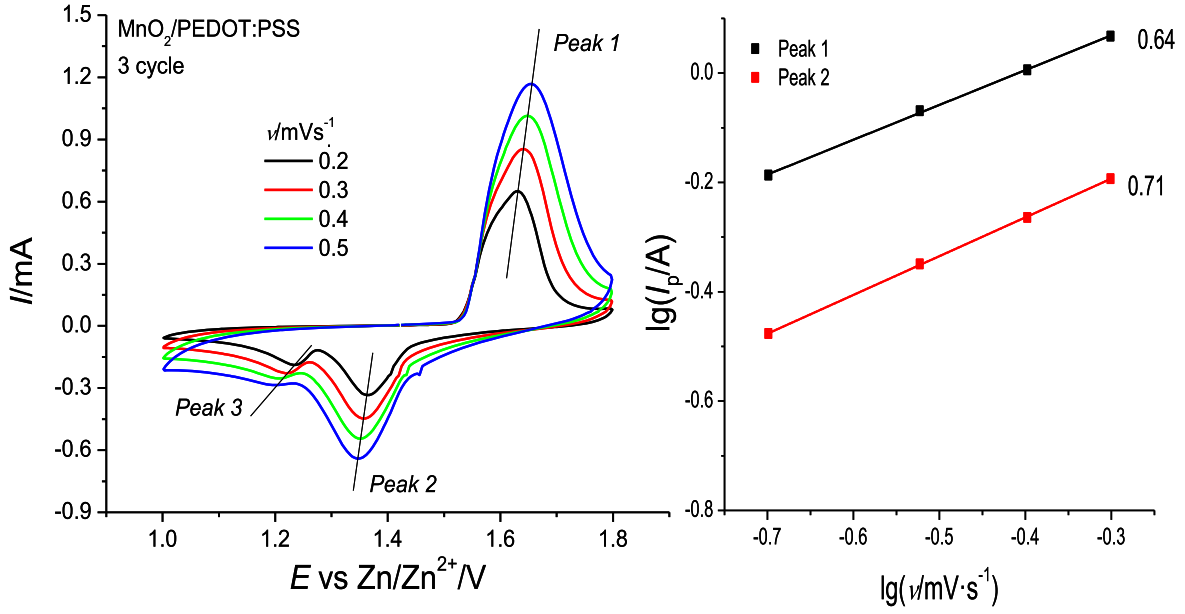

Figure 4. (a) Cyclic voltammograms of MnO_2/PEDOT:PSS electrode at different scan rates; (b) double logarithmic dependencies of peak current on scan rate for MnO_2/PEDOT:PSS electrode.

$$(\log I_p) = \log a + b \cdot \log \nu \qquad [2]$$

When the b value is close to 0.5, it is suggested that ion diffusion limits the current of the electrochemical process, b value close to 1.0 correspond to (pseudo)capacitive response. Thus, insertion and extraction of protons is controlled dominantly by diffusion of H^+-ions and it may influence the pH value near the electrode surface with contributions from a pseudocapacitive response. Because of formation of the excess of OH^--anions, the formation of zinc hydroxyl sulfate takes place during discharge process. This mechanism is in agreement with reported ones intensively discussed.[25,26]

Electrochemical performance of the MnO_2-based cathodes is presented on Fig. 5. At low current densities increase of specific capacity can be explained by MnO_x (ε-MnO_2) layer formation on the electrode surface. In case of PEDOT:PSS-coated electrode capacity values (over 300 mAh g^{-1} at low current densities) are approaching the theoretical value until current density 1.0 $A{\cdot}g^{-1}$ and are much higher at the last cycles at 0.1 $A{\cdot}g^{-1}$ due to additional formation of electroactive layer MnO_x formed on the electrode and in spaces at $E = 1.7$ V and higher where a visible dark precipitate was observed. At high current density (5.0 $A{\cdot}g^{-1}$) all three electrode materials delivered zero capacity.

During long-term cycling capacity increases in initial cycles at 0.1 $A{\cdot}g^{-1}$, and in following 20–30 cycles at 0.3 $A{\cdot}g^{-1}$ a capacity

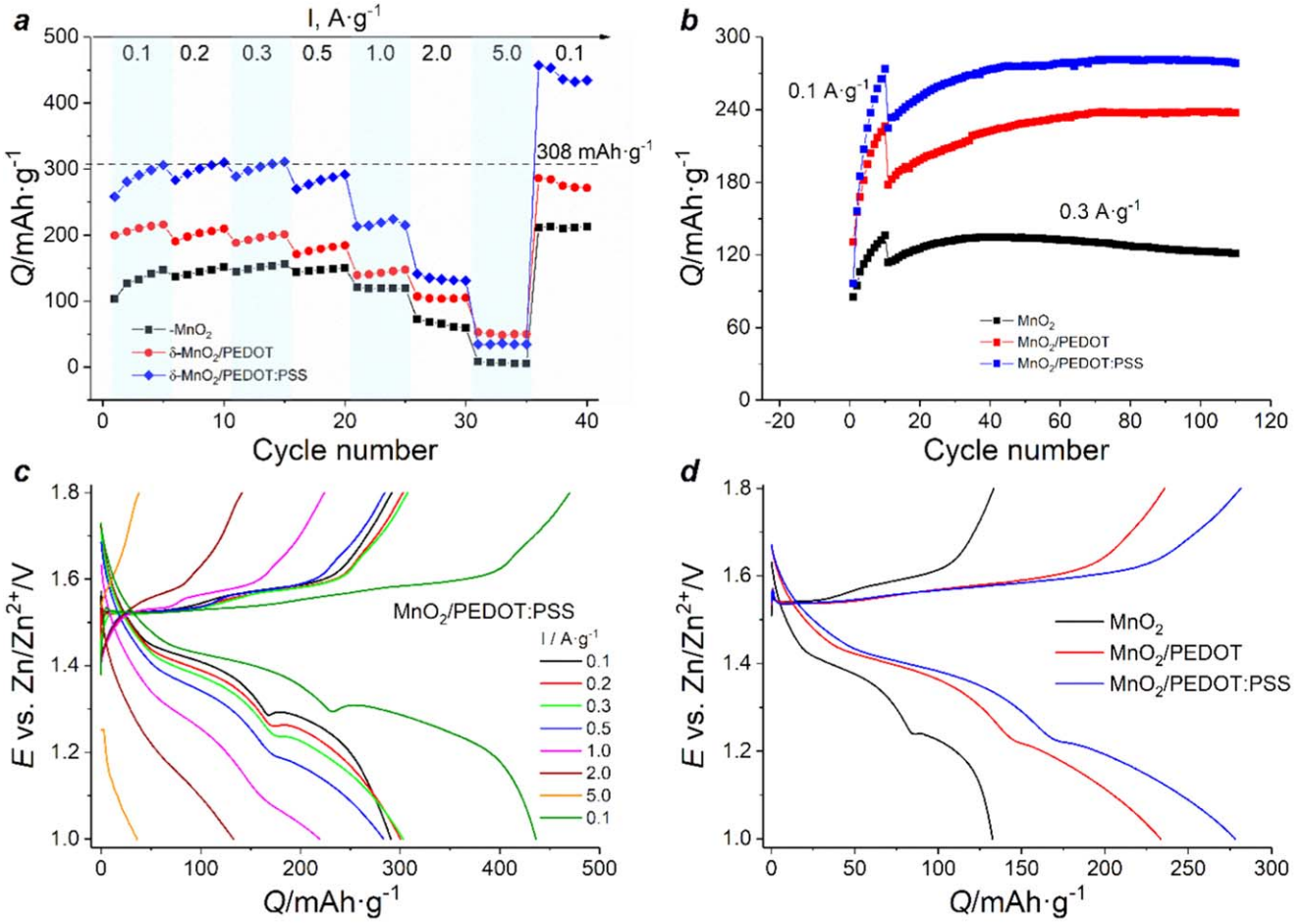

Figure 5. Electrochemical performance of δ-MnO_2-based electrodes: C-rate capabilities (a); cycling stability at 0.3 $A \cdot g^{-1}$ (b). GCD curves of MnO_2/PEDOT:PSS electrode at different current densities (c) and at 0.3 $A \cdot g^{-1}$ (d).

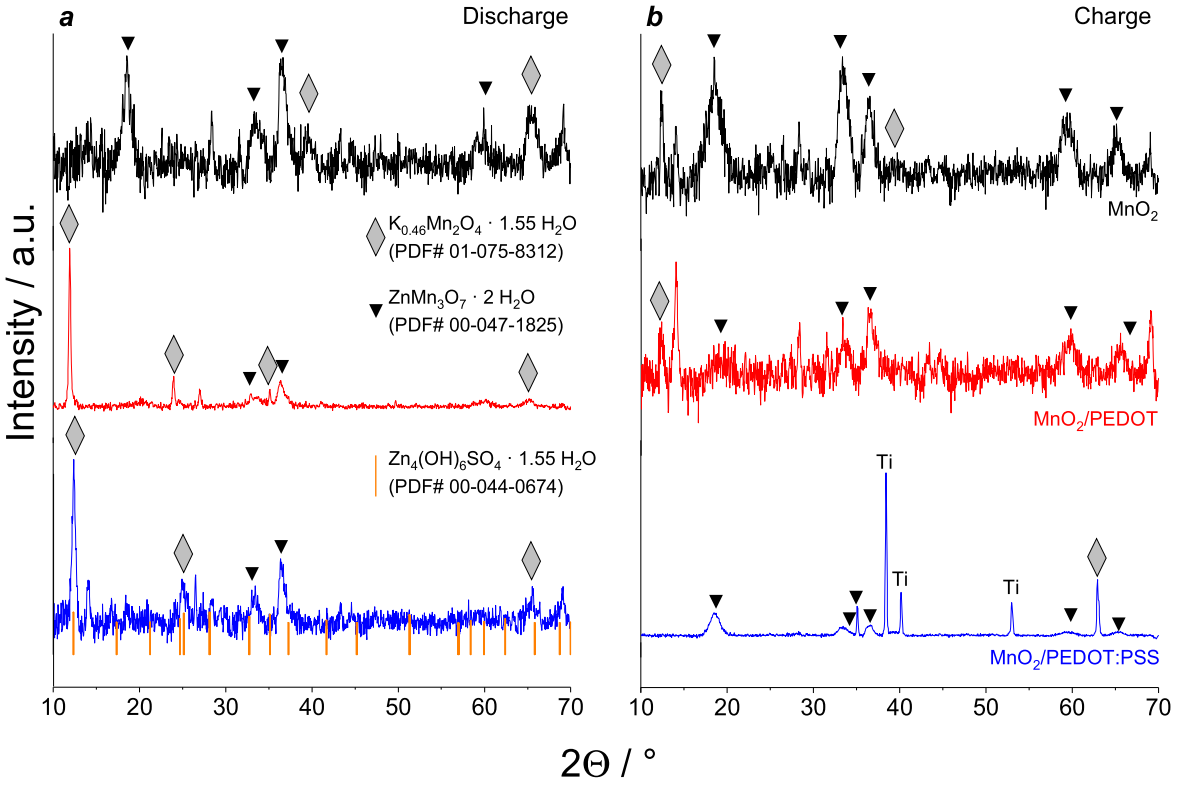

Figure 6. XRD patterns of MnO_2-based electrodes after electrochemical tests in discharged (a) and charged (b) states.

increase of 15% for MnO_2, 25% for MnO_2/PEDOT and 20% for MnO_2/PEDOT:PSS electrodes is observed (Fig. 5b). Furthermore for pristine δ-MnO_2 cathode capacity decrease by 10% while for modified electrodes no capacity fading is observed after stabilization (capacity retention from maximum value is 90% for MnO_2, 99.5% for MnO_2/PEDOT and 99% for MnO_2/PEDOT:PSS). Capacity values of PEDOT:PSS-coated electrode materials are twice higher than for MnO_2-based electrode which can be associated with increased electronic conductivity of composite material and, as a consequence, fast ion transport between electroactive grains. These values are also on par with the other state-of-the-art manganese-based cathodes for aqueous zinc-ion batteries (see Table SIII).

Charge/discharge profiles of all types of electrodes (Fig. 5d) show one long charge plateau close to 1.55 V and two discharge plateaus at 1.4 and 1.25 V. It is clearly seen on the discharge curves that the plateau at E = 1.4 V is a bit longer than the second one, which allows to suggest that proton intercalation is dominant energy storage process instead of Zn^{2+}-ion intercalation. On the discharge curves (Figs. 5c, 5d) at $E = 1.26$–1.28 V an increase of the potential is detected. It corresponds to zinc ion intercalation or/and chemical precipitation of a Zn^{2+}-containing insoluble byproduct zinc sulfate hydroxide. In the presence of the ICP the slope of the curve at the end is smoother than for pristine MnO_2-based cathode (Fig. 5d) which is associated with the shape of CV curves of MnO_2/PEDOT and MnO_2/PEDOT:PSS electrodes during discharge process.

For detailed investigation of structural changes in the electrode material, XRD patterns of MnO_2-based cathodes were obtained after 100 charge/discharge cycles in charged and discharged states (Fig. 6). In discharged state for bare MnO_2-based electrode, the main diffraction peaks of δ-MnO_2 (ICCD card no. 01–75–8312, gray symbols) stay and additional strong peaks at 18.55°, 33.67°, 36.59° and 65.39° (noted as black symbols) are observed. These peaks are associated with Zn-doped manganese dioxide $ZnMn_3O_7{\cdot}2\ H_2O$ (ICCD card no. 00–047–1825). It should be noted that several peaks (12.35°, 25.14°, 32.75°, 35.12 °) are wider due to the presence of highly amorphous phase $Zn_4(OH)_6SO_4{\cdot}1.55\ H_2O$ (ZHS) matching the ICCD card no. 00–044–0674. For electrodes with ICP diffraction peaks of Zn-doped manganese oxide are smaller, so we can conclude that PEDOT or PEDOT:PSS prevents the active irreversible zinc ion insertion in the electrode material lattice.

In the charged state (Fig. 6b) peaks related to ZHS phase are not noticed, so we can conclude that additional surface layer of ZHS dissolves during charge process in agreement with the data presented in Ref. 23. The main crystal phase is Zn-doped hydrated oxide $ZnMn_3O_7$ while the pristine MnO_2 phase almost disappeared. So, irreversible insertion of Zn^{2+} ions in crystal lattice is also confirmed during charge process.

Conclusions

A comparative electrochemical study of δ-MnO_2-based electrodes modified by PEDOT additive or PEDOT:PSS coating was performed. It was shown that addition of PEDOT and especially PEDOT:PSS leads to an increase of specific capacities: the values delivered were 243 and 219 $mAh{\cdot}g^{-1}$ at 1.0 $A{\cdot}g^{-1}$ while only 119 $mA{\cdot}g^{-1}$ was obtained for bare δ-MnO_2 electrode. At low current densities capacity values of MnO_2/PEDOT:PSS electrodes are comparable with the theoretical values for MnO_2 cathodes for AZIBs. The cycling stability of both electrodes modified by ICPs during 100 cycles was close to 99%. The significant increase of specific capacity during cycling is linked with additional formation of ε-MnO_2 layer on the electrode surface.

Enhancing the electrochemical properties of MnO_2 cathodes with conducting polymers can be explained by the increase of both electronic and ionic conductivity of electrode material due to more conductive media between electroactive grains. In addition, a polymer layer on the electrode surface (in case of PEDOT:PSS coating) supports the mechanical integrity and prevents the manganese dissolution during charge/discharge processes. It follows from the experimental data, that addition of the ICP to electrode slurry in form of dispersion of PEDOT with polystyrene sulfonate anion (PEDOT:PSS) was better than of PEDOT only. This can be explained by assuming a more homogeneous and tight thin layer coating of active grains by PEDOT:PSS, facilitating surface electronic and ionic conductivity, which enhances the rate capability and cycling performance. Moreover, PEDOT:PSS as tight thin layer coating supports more reliable electrical contacts between inorganic active species and carbon species, reducing the interfacial Ohmic resistance.

Investigation of the redox processes shows that the introduction/extraction of protons is the dominant process at high current densities (or short charge/discharge times) based on diffusion-controlled currents. This leads to a local increase in pH and the precipitation of zinc hydroxyl sulfate (ZHS) on the electrode surface, inhibiting the zinc ion insertion reaction.

Acknowledgments

The financial support from Russian Foundation for Basic Research (grant № 21–53–53012) is gratefully acknowledged. Materials characterization was performed at the Center for X-ray Diffraction Studies and the Interdisciplinary Center for Nanotechnology of Research Park of St. Petersburg State University.

ORCID

R. Holze https://orcid.org/0000-0002-3516-1918

References

1. H. Liu, J. G. Wang, Z. You, C. Wei, F. Kang, and B. Wei, *Mater. Today*, **42**, 73 (2021).
2. X. Zhang, L. Wang, and H. Fu, *J. Power Sources*, **493**, 229677 (2021).
3. D. Selvakumaran, A. Pan, S. Liang, and G. Cao, *J. Mater. Chem. A*, **7**, 18209 (2019).
4. L. Chen, Q. An, and L. Mai, *Adv. Mater. Interfaces*, **6**, 1900387 (2019).
5. V. Mathew et al., *ACS Energy Lett.*, **5**, 2376 (2020).
6. X. Guo, S. Yang, D. Wang, A. Chen, Y. Wang, P. Li, G. Liang, and C. Zhi, *Curr. Opin. Electrochem.*, **30**, 100769 (2021).
7. Z. Zhang, W. Li, Y. Shen, R. Wang, H. Li, M. Zhou, W. Wang, K. Wang, and K. Jiang, *J. Energy Storage*, **45**, 103729 (2022).
8. C. Guo, H. Liu, J. Li, Z. Hou, J. Liang, J. Zhou, Y. Zhu, and Y. Qian, *Electrochim. Acta*, **304**, 370 (2019).
9. M. H. Alfaruqi, J. Gim, S. Kim, J. Song, D. T. Pham, J. Jo, Z. Xiu, V. Mathew, and J. Kim, *Electrochem. Commun.*, **60**, 121 (2015).
10. L. Tang, X. Ji, H. Luo, M. Yao, and S. Cheng, *J. Alloys Compd.*, **834**, 155117 (2020).
11. V. Soundharrajan, B. Sambandam, S. Kim, S. Islam, J. Jo, S. Kim, V. Mathew, Y.-K. Sun, and J. Kim, *Energy Storage Mater.*, **28**, 407 (2020).
12. J. Huang, X. Tang, K. Liu, G. Fang, Z. He, and Z. Li, *Mater. Today Energy*, **17**, 100475 (2020).
13. C. Guo, S. Tian, B. Chen, H. Liu, and J. Li, *Mater. Lett.*, **262**, 127180 (2020).
14. J. Huang, Z. Wang, M. Hou, X. Dong, Y. Liu, Y. Wang, and Y. Xia, *Nat. Commun.*, **9**, 1 (2018).
15. P. Ruan et al., *Sustain. Mater. Technol.*, **28**, e00254 (2021).
16. Y. Zeng, X. Zhang, Y. Meng, M. Yu, J. Yi, Y. Wu, X. Lu, and Y. Tong, *Adv. Mater.*, **29**, 1700274 (2017).
17. X. Zhang, S. Wu, S. Deng, W. Wu, Y. Zeng, X. Xia, G. Pan, Y. Tong, and X. Lu, *Small Methods*, **3**, 1900525 (2019).
18. M. A. Kamenskii, S. N. Eliseeva, and V. V. Kondratiev, *ECS Trans.*, **105**, 135 (2021).
19. F. Zhang, C. Wang, J. Pan, F. Tian, S. Zeng, J. Yang, and Y. Qian, *Mater. Today Energy*, **17**, 100443 (2020).
20. D.-S. Liu, Y. Mai, S. Chen, S. Liu, E. H. Ang, M. Ye, Y. Yang, Y. Zhang, H. Geng, and C. C. Li, *Electrochim. Acta*, **370**, 137740 (2021).
21. W. Zhou, A. Wang, A. Huang, M. Chen, Q. Tian, J. Chen, and X. Xu, *Front. Energy Res.*, **8**, 182 (2020).
22. X. Guo, J. Zhou, C. Bai, X. Li, G. Fang, and S. Liang, *Mater. Today Energy*, **16**, 100396 (2020).
23. A. O. Efremova, A. I. Volkov, E. G. Tolstopyatova, and V. V. Kondratiev, *J. Alloys Compd.*, **892**, 162142 (2022).
24. Y. Jin et al., *Adv. Mater.*, **31**, 1900567 (2019).
25. C. F. Bischoff, O. S. Fitz, J. Burns, M. Bauer, H. Gentischer, K. P. Birke, H.-M. Henning, and D. Biro, *J. Electrochem. Soc.*, **167**, 020545 (2020).
26. Y. Tan, F. An, Y. Liu, S. Li, P. He, N. Zhang, P. Li, and X. Qu, *J. Power Sources*, **492**, 229655 (2021).